applied sciences

MDPI

Article

Investigation on Double-Deck Vibratory Screening of Shield Muck in Moderately Weathered Strata Using EDEM Simulation and Multi-Factor Analysis

Yong Yu [1], Xiaoyu Wang [2,*], Weiguo He [1], Yang Luo [2], Tengfei Li [1], Wenjun Liu [1], Yijie Zhang [2,*] and Fei Liu [2]

[1] China Railway Liuyuan Group Corporation Limited, Tianjin 300308, China
[2] School of Qilu Transportation, Shandong University, Jinan 250061, China
* Correspondence: xywang0321@163.com (X.W.); jjzyjie@126.com (Y.Z.)

Abstract

The shield tunneling method is widely used for underground space development in the world, where vibratory screening is a critical pretreatment stage for resource utilization of shield muck. However, existing parameters for vibrating screens are mainly based on soft soil and sandy cobblestone strata. Research regarding shield muck from moderately weathered strata remains scarce, leading to poor equipment adaptability and low efficiency. This study focuses on a dry granular system of typical shield muck from moderately weathered strata after washing, drying, and homogenization. By combining laboratory standard sieve tests with EDEM discrete element simulations, a DEM numerical model of double-deck vibratory screening was established. Using single-factor controlled variables and orthogonal experimental designs, the comprehensive influences of vibration frequency, amplitude, and screen inclination angle on a double-deck screen were systematically investigated. Within the investigated parameter ranges, the screen inclination angle produced a relatively large variation in screening efficiency. Based on the preliminary evaluation using the numerical model developed in this study, a vibration frequency of 15 Hz, an amplitude of 2.0 mm, and a screen inclination angle of 12° exhibited favorable overall screening performance among the investigated parameter combinations, yielding upper- and lower-deck screening efficiencies of 95.16% and 82.96%, respectively. The results indicate that changes in the feed state of the lower deck induced by upper-deck pre-classification may be associated with the differentiated responses of the two screen decks to operating parameters, providing a reference for multi-stage screening analysis and parameter selection for shield muck from moderately weathered strata.

Keywords: shield muck; moderately weathered strata; vibratory screening; discrete element method; screening efficiency

Check for updates

Academic Editor: Sungchul Yang

Received: 7 September 2026
Revised: 23 October 2026
Accepted: 23 October 2026
Published: 26 October 2026

Copyright: © 2026 by the authors. Licensee MDPI, Basel, Switzerland. This article is an open access article distributed under the terms and conditions of the Creative Commons Attribution (CC BY) license.

1. Introduction

With the accelerated construction of major infrastructures such as urban subways and cross-river tunnels in China, the shield tunneling method has become the mainstream technique for underground space development due to its advantages of high construction efficiency and minimal disturbance to the surrounding environment [1]. However, the disposal of vast amounts of shield muck generated during construction has emerged as a bottleneck restricting the green and sustainable development of engineering projects. The volume of muck produced by a single shield tunnel can reach hundreds of thousands

of cubic meters. Due to uneven weathering degrees in moderately weathered strata, the corresponding shield muck exhibits a wide grain-size distribution span and significant fluctuations in mud content. Furthermore, the muck often contains residual additives such as bentonite and surfactants, making its treatment far more challenging than that of ordinary soft soil or sandy cobblestone muck. If randomly stockpiled without effective treatment, it not only occupies extensive land resources but also triggers ecological and environmental risks, including landslides and groundwater pollution [2,3]. Vibratory screening is an essential pretreatment stage for the resource-oriented conditioning and utilization of shield muck, with its core functions being particle size classification and impurity separation. Hatefi et al. [4] systematically reviewed the effects of particle shape on the mechanical behavior of granular materials, highlighting particle morphology as an important factor influencing particle motion and contact characteristics. Yang et al. [5] systematically reviewed DEM-based vibratory screening technologies and research methods, summarizing the effects of particle motion, screening mechanisms, and operating parameters on screening performance.

Compared with muck generated in ordinary soft-soil or sandy gravel strata, muck from moderately weathered strata exhibits a wider particle size distribution and more pronounced fluctuations in clay content because of the uneven degree of weathering. Moreover, residual construction additives, such as bentonite and surfactants, often increase its cohesiveness, making it susceptible to particle agglomeration and screen aperture blockage. These characteristics consequently reduce screening efficiency, impair classification accuracy, and disrupt production continuity. Meanwhile, conventional physical-test-based optimization methods are costly and time-consuming, making it difficult to systematically investigate the variations in particle migration and screening performance under the combined effects of multiple factors. Guo et al. [6] employed a coupled CFD–DEM–FEM method to investigate the double-deck vibratory screening process of slurry shield muck and analyzed the screening characteristics under multi-field coupling effects. Jaiswal et al. [7] investigated particle stratification during vibratory screening using DEM, revealing the effects of different operating conditions on particle stratification and penetration behavior. Zhang et al. [8] investigated the effects of vibration frequency and amplitude on screening performance and achieved the coordinated optimization of screening efficiency and screen surface load. Niu et al. [9] conducted fault diagnosis research on the screen mesh of mining vibrating screens, enabling the identification and classification of abnormal screen mesh conditions.

The discrete element method (DEM) calculates particle–particle and particle–boundary contact interactions, thereby enabling the particle-scale characterization of collision, stratification, transportation, and penetration during the screening of bulk materials. It has thus become an important numerical method for investigating vibratory screening processes. In recent years, DEM-based research has gradually expanded from conventional screening simulations to complex vibration trajectories, the screening of wet and cohesive particles, multi-deck screening, flexible screen deck coupling, and multi-parameter optimization. Geng et al. [10] used DEM to compare the effects of external moisture content on the screening performance of vibrating flip-flow and circular vibrating screens, revealing its influence on particle motion and particle size distribution. Yang and Ma [11] developed a discrete element model of a composite vibrating screen and investigated the effects of composite vibration trajectories on material transportation and screening efficiency in terms of particle forces, stratification, and throwing motion. Zhou et al. [12] combined DEM with the grey wolf optimization algorithm and support vector regression to investigate the nonlinear relationships between the screening parameters and performance of wet gravel. Zhang et al. [13] employed DEM and a PSO–BP neural network to analyze the parameter

responses of a multi-angle vibrating screen and achieve the coordinated optimization of vibration parameters. Li et al. [14] developed a surrogate model for a three-deck vibrating screen, analyzed the effects of multiple vibration parameters on the screening performance of each deck, and optimized these parameters. Xu et al. [15] established a coupled DEM–FEM–MBD model to characterize the dynamic interactions between particulate materials and a flexible screen deck and optimized the operating parameters of a vibrating flip-flow screen. Collectively, these studies demonstrate that DEM-based vibratory screening research is evolving from single-parameter analyses of rigid screen decks toward the modeling of complex materials, multi-deck screening, flexible screen deck coupling, and intelligent multi-parameter optimization.

Although substantial progress has been made in vibration modes, screen deck structures, and parameter optimization, existing studies have still mainly focused on conventional bulk materials such as coal, ore, and gravel, with most attention directed toward single-deck screening, specific vibration trajectories, or multi-parameter optimization. The evolution of particle states between different screen decks and the transfer of screening performance during multi-deck screening remain relatively insufficiently understood. In contrast, shield muck from moderately weathered strata is characterized by a wide particle size distribution, complex composition, and a high proportion of fine particles. Its double-deck screening process sequentially involves upper-deck retention and penetration, inter-deck migration, lower-deck secondary screening, and classified discharge. The selective retention and penetration on the upper screen deck further alter the particle size composition, quantity distribution, and motion state of the feed entering the lower deck. Therefore, lower-deck screening is not a simple repetition of the upper-deck process, but is jointly influenced by upper-deck pre-classification and inter-deck migration.

At present, the continuous evolutionary process of "upper-deck pre-classification–inter-deck migration–lower-deck secondary screening" remains insufficiently understood. In particular, how the changes in particle states induced by upper-deck screening further affect the screening performance of the lower deck, and why the upper and lower screen decks exhibit different responses to the same operating parameters, have not yet been fully revealed. In addition, when vibration frequency, amplitude, and screen inclination angle act simultaneously, complex competitive relationships arise among particle transportation, material-bed loosening, and effective opportunities for penetration, and their effects on the screening performance of the upper and lower decks also differ markedly. Therefore, the inter-deck evolution of particle states and the differentiated parameter responses during double-deck screening of shield muck with a complex and wide particle size distribution remain scientific issues that require further investigation. Unlike existing multi-deck screening studies that mainly focus on screening performance, parameter optimization, and particle separation behavior, this study treats double-deck screening as a continuous particle evolution process characterized by inter-deck state transfer, with particular emphasis on the changes in particle states induced by upper-deck pre-classification and their relationship with the subsequent screening response of the lower deck.

To address the above scientific issues, this study focuses on shield muck from moderately weathered strata and establishes a numerical model of double-deck vibratory screening by combining laboratory particle size distribution tests with EDEM discrete element simulations. First, the particle-scale motion and classification characteristics of the muck during upper-deck screening, inter-deck migration, and lower-deck secondary screening are analyzed to clarify the migration paths of particles with different size fractions between the upper and lower screen decks. Second, single-factor analyses are conducted to investigate the differentiated effects of vibration frequency, amplitude, and screen inclination angle on the screening performance of the upper and lower decks, and the response

characteristics of the two screen decks are interpreted in conjunction with particle motion states. Furthermore, multi-factor experiments are performed to compare the variations in double-deck screening performance under different parameter combinations and to determine a suitable parameter combination under the conditions investigated in this study.

This study focuses on the particle-state reconfiguration induced by upper-deck preclassification and its influence on the subsequent screening response of the lower deck, aiming to establish a particle-scale understanding of the "upper-deck screening–inter-deck state reconfiguration–differentiated lower-deck response" process for shield muck with a wide particle size distribution. The results can not only deepen the understanding of the interrelationship between successive screening stages during double-deck screening, but also provide a reference for multi-stage screening studies of similar wide-size-range bulk materials and for the rational configuration of screening parameters for shield muck from moderately weathered strata. The framework is illustrated in Figure 1.

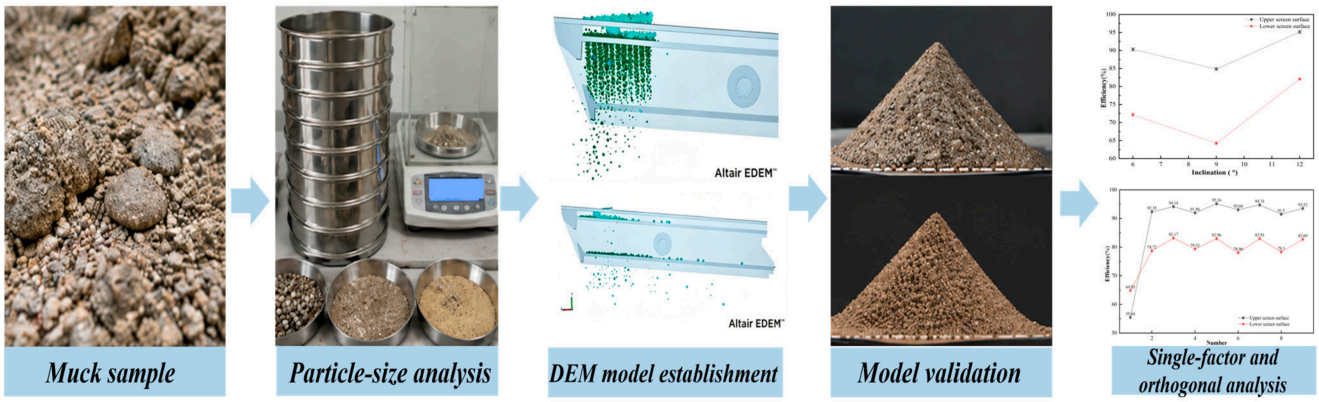


Figure 1. Research framework and main workflow of this study.

2. Characterization of Shield Muck Properties

The shield muck samples used in this study were collected from the construction site of Honglou Square Station on Jinan Metro Line 7, where the sampled stratum primarily consisted of moderately weathered diorite. The collected muck samples were sealed and transported to the laboratory for subsequent particle size distribution measurements and screening tests. The particle size distribution characteristics of the muck were determined through size-fraction screening, providing an experimental basis for setting the particle sizes in the subsequent discrete element model.

2.1. Physical Characterization of Shield Muck

The material used in this experiment was shield tunneling muck derived from moderately weathered strata, which had undergone primary washing, drying, and homogenization in the laboratory. The processed muck exhibited no obvious agglomeration, impurities, or oversized debris, and the overall particle distribution was relatively uniform, making it suitable for screening tests. The sample reflects the particle size distribution characteristics of shield muck from the moderately weathered strata of the case project after washing, drying, and homogenization, providing a field-derived material basis for setting the particle sizes and mass proportions in the subsequent numerical model. In this experiment, the muck specimen was sampled using the quartering method, and a final mass of approximately 500 g was weighed as the sample for the screening test. After being transported to the laboratory, the shield muck samples were first washed to remove impurities adhering to the particle surfaces, followed by drying at 105 °C for 3 h and homogenization. The processed samples were subsequently used for particle size distribution

measurements. It should be noted that the washing process may have resulted in the loss of a small amount of ultrafine particles. Therefore, the particle size distribution obtained in this study primarily reflects the particle size composition of the muck after pretreatment.

The apparatus utilized in this screening test was a set of standard square-hole test sieves. All sieve meshes complied with the relevant stipulations of the standard GB/T 6003.1 [16]. The sieve frames were constructed of stainless steel, and the meshes were made of woven wire with standard square openings. The equipment was in excellent condition, with no damage or deformation observed in the meshes, thereby satisfying the requirements for experimental precision.

The sieve set comprised seven levels of standard sieves with different apertures and one solid bottom pan. From top to bottom, the sieve opening sizes were sequentially 9.50 mm, 4.75 mm, 2.36 mm, 1.18 mm, 0.6 mm, 0.3 mm, and 0.15 mm. This configuration completely covered the particle size distribution range of the muck, enabling graded screening from coarse to fine particles. Prior to the test, the sieves were stacked in descending order of aperture size, with the solid bottom pan fitted at the base to ensure that the fine materials could be fully collected during the screening process. The experimental flowchart is illustrated in Figure 2.

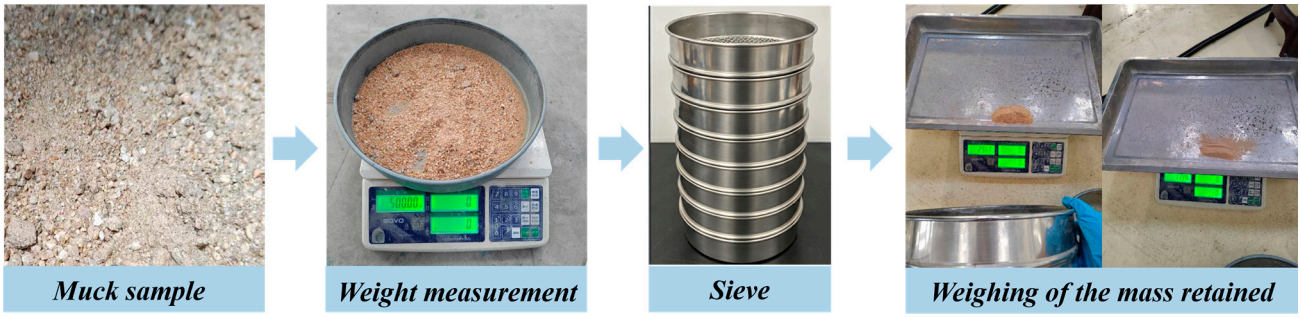


Figure 2. Flowchart of the laboratory standard sieve test for shield muck.

(1) The stacked sieve assembly was placed horizontally on the laboratory bench, ensuring that the sieve frames fitted tightly together without any discernible gaps.
(2) The weighed 500 g muck specimen was poured onto the uppermost sieve deck with a 9.50 mm aperture.
(3) Holding the sieve frames with both hands, the screening process was executed via horizontal reciprocation combined with slight vertical vibration. The screening intensity was carefully regulated during the process to ensure that the material was fully loosened and stratified on the screen surfaces, thereby providing sufficient time for fine particles to pass through the mesh.
(4) The screening duration for each sieve level was maintained for no less than 3 min. Once no significant amount of material was observed passing through the openings, the sieves were detached sequentially to collect the retained material on each screen deck and the undersize material in the bottom pan.
(5) Upon completion of the screening process, each sieve level and the bottom pan were thoroughly cleaned, and the mass of the retained material on each sieve was weighed for statistical analysis of the experimental data. The laboratory screening test was independently repeated three times, and the masses of each particle size fraction and the corresponding gradation parameters were determined by averaging the results of the three tests.

2.2. Analysis of Screening Test Results

Upon completion of the experiment, the retained material on each sieve deck was weighed and statistically analyzed to obtain the mass distribution of the shield muck across different particle size intervals; the results are tabulated in Table 1. Furthermore, the particle size distribution curve of the experimental muck, derived by calculating the cumulative passing percentage of each sieve aperture, is illustrated in Figure 3.

Table 1. Particle size distribution of shield muck from screening tests.

Sieve Size (mm)	Mass Retained (g)	Individual Retained (%)	Cumulative Retained (%)	Cumulative Passing (%)
9.50	2.17	0.43	0.43	99.57
4.75	3.48	0.70	1.13	98.87
2.36	161.79	32.34	33.47	66.53
1.18	126.40	25.27	58.74	41.26
0.60	77.08	15.41	74.15	25.85
0.30	88.37	17.66	91.81	8.19
0.15	29.67	5.93	97.74	2.26
Bottom	11.44	2.26	100.00	-

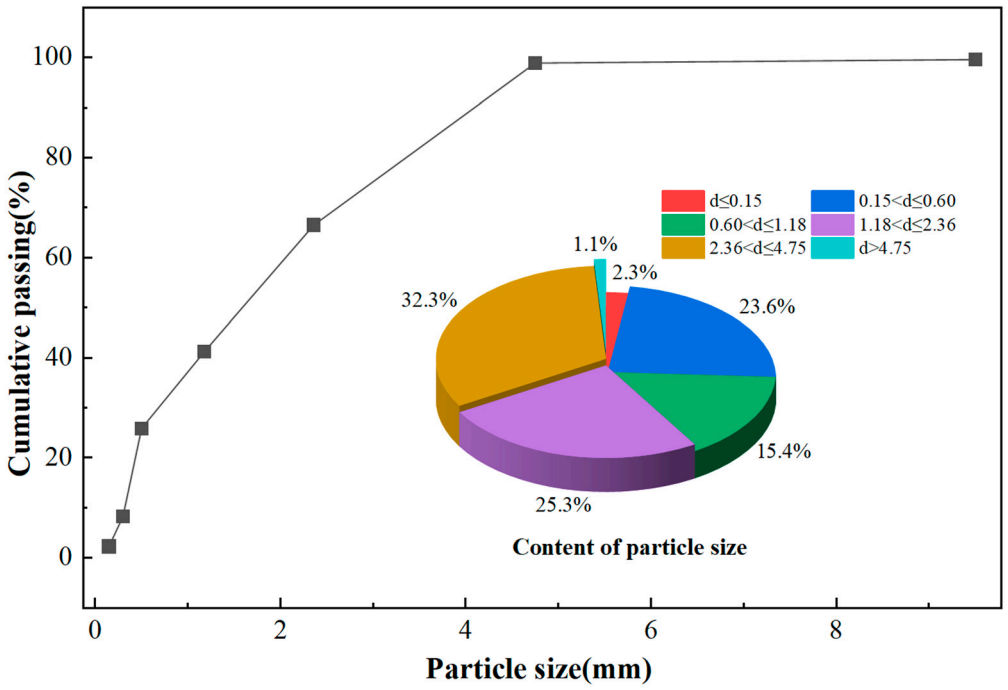


Figure 3. Particle size distribution curve of the experimental shield muck.

The coefficient of uniformity C_u and the coefficient of curvature C_c are two crucial indicators for evaluating particle size distribution. Their calculation formulas are expressed as follows:

$$C_u = \frac{d_{60}}{d_{10}} \quad (1)$$

$$C_c = \frac{d_{30}^2}{d_{10} \cdot d_{60}} \quad (2)$$

where d_{10} is the effective particle size, which corresponds to the particle diameter at 10% cumulative percentage passing on the particle size distribution curve; d_{30} is the particle diameter at 30% cumulative percentage passing on the curve; and d_{60} is the constrained

particle size, which represents the particle diameter at 60% cumulative percentage passing. The experimental results are tabulated in Table 2:

Table 2. Soil grading parameters of the experimental muck.

	d_{10} (mm)	d_{30} (mm)	d_{60} (mm)	C_u	C_c
Result	0.32	0.90	1.97	6.16	1.28

The calculation results demonstrate that the coefficient of uniformity C_u of the shield muck from the moderately weathered strata used in the test is greater than 5, indicating a wide range of particle size distribution and a prominent gradient between coarse and fine particles. The coefficient of curvature C_c ranges between 1 and 3, implying an appropriate content of medium-sized particles, a continuous and smooth grading curve, and the absence of missing particle sizes or grading gaps, thereby ensuring a stable transition across all particle fractions. Comprehensive evaluation of both indicators confirms that the soil is well-graded. The particle size distribution described above reflects the actual gradation characteristics of shield muck from the moderately weathered strata at Honglou Square Station on Jinan Metro Line 7, providing a field-test basis for setting the particle sizes and their proportions in the subsequent EDEM model. The particle size composition of shield muck is influenced by factors such as stratum lithology, degree of weathering, tunneling parameters, and muck conditioning measures. Therefore, the gradation characteristics and screening results obtained in this study are primarily applicable to shield muck with geological conditions and material compositions similar to those of the case project.

3. EDEM-Based Simulation of the Vibrating Screening Process

3.1. Development of the Discrete Element Simulation Model

3.1.1. Fundamentals of EDEM Simulation

The DEM is a discontinuous medium numerical simulation approach based on Newton's second law and contact mechanics theory [17,18]. Its core principle is to discretize poorly continuous bulk materials into a multitude of independent, mobile, and mutually colliding rigid or deformable particle elements. By solving the governing dynamic equations of each particle under contact and external forces via time-step iterations, the positions, velocities, force states, and motion postures of all particles are updated progressively over time. This approach ultimately solves the macroscopic motion and mechanical behavior of the particle system across the entire domain, fully replicating the dynamic evolutionary process of the material. Traditional continuum mechanics methods, such as the finite element method (FEM), are premised on assumptions of homogeneity, continuity, and isotropy; hence, they are exclusively applicable to solid materials with strong integrity and continuous deformation, such as rocks and metals. In contrast, shield muck is a typical heterogeneous multi-phase bulk material comprising various components, including soil, sand, gravel, and impurities, which features high porosity and unstable cohesion properties. During the vibratory screening process, it is highly prone to discontinuous and nonlinear mechanical behaviors, such as loose slippage, particle segregation, localized accumulation, aperture clogging, and bounding penetration. Continuum methods fail to precisely capture these microscopic dynamic characteristics between individual particles, leading to substantial deviations between simulation outcomes and actual working conditions. Compared with these limitations, DEM abandons the continuity assumption of the medium and fully accounts for the independence and contact randomness of bulk particles [19,20]. Consequently, it can replicate the full dynamic process of shield muck on a vibrating screen surface from a microscopic particle scale while accurately quantifying

key motion parameters, rendering it the optimal numerical method currently available for the screening simulation of discontinuous, multi-phase, and mixed bulk materials. This study employs EDEM discrete element simulation software to investigate the vibratory screening process of shield muck. Previous studies have demonstrated that different DEM numerical frameworks can be used to simulate bulk particle processes [21]. Furthermore, the Hertz–Mindlin contact model in EDEM was adopted to characterize particle–particle and particle–screen deck contact interactions [22,23]. By constructing rational particle models and establishing accurate contact parameters, the vibratory screening process of shield muck was simulated to predict and analyze screening performance under various operating conditions.

3.1.2. Contact Model

In EDEM discrete element simulations, the contact behavior between particles is defined by the contact model, and its selection directly dictates the correlation between simulation results and actual working conditions. Tailored to the mechanical properties of the shield muck from the moderately weathered strata, the Hertz-Mindlin (no-slip) contact model was selected as the core contact model in this study. Based on the Hertz contact theory and the Mindlin-Deresiewicz slip theory, this model simultaneously calculates the normal contact force and tangential friction force between particles, thereby accurately characterizing the contact mechanical behavior of the shield muck particles.

Assuming that spherical particle 1 and spherical particle 2 undergo an elastic collision, the normal overlap between the two particles is denoted as α. In the normal direction, the Hertz contact theory posits that the contact area undergoes elastic contact, and the normal force exhibits a nonlinear relationship with the contact deformation. Its calculation formula is expressed as follows:

$$F_n = \frac{4}{3} E^* (R^*)^{\frac{1}{2}} \alpha_n^{\frac{3}{2}} \tag{3}$$

where E^* is the equivalent elastic modulus, and its calculation formula is expressed as follows:

$$\frac{1}{E} = \frac{1-\nu_1^2}{E_1} + \frac{1-\nu_2^2}{E_2} \tag{4}$$

where E_1 and E_2 are the elastic moduli of spherical particle 1 and spherical particle 2, respectively; and ν_1 and ν_2 are the Poisson's ratios of spherical particle 1 and spherical particle 2, respectively.

In Equation (5), R^* is the equivalent radius when the two spherical particles are in contact, and its calculation formula is expressed as follows:

$$\frac{1}{R^*} = \frac{1}{R_1} + \frac{1}{R_2} \tag{5}$$

where R_1 and R_2 are the radii of the two spheres.

In the tangential direction, the Mindlin-Deresiewicz theory accounts for tangential interactions during particle contact, where the tangential elastic force can be expressed as follows:

$$F_t = -8G^* \sqrt{R^* \alpha_n} \delta_t \tag{6}$$

The tangential damping force is calculated using the Hertz–Mindlin (no-slip) contact model in EDEM based on the relative tangential velocity between particles and the coefficient of restitution.

where G^* is the equivalent shear modulus, and its calculation formula is expressed as follows:

$$\frac{1}{G} = \frac{2-\nu_1}{G_1} + \frac{2-\nu_2}{G_2} \tag{7}$$

where G_1 and G_2 are the shear moduli of spherical particle 1 and spherical particle 2, respectively.

In Equation (6), δ_t represents the accumulated tangential displacement during particle contact, which is used to calculate the tangential elastic force under the current contact state. The tangential displacement increment between two adjacent computational time steps is denoted as $\Delta\delta_t$, and its calculation formula is expressed as follows:

$$\Delta\delta_t = u_t^{(i)} - u_t^{(i-1)} \tag{8}$$

where $\Delta\delta_t$ represents the tangential displacement increment between two adjacent computational time steps, and $u_t^{(i)}$ and $u_t^{(i-1)}$ represent the relative tangential displacements at the particle contact point in the current and previous time steps, respectively.

3.1.3. Simulation Settings

A 3D geometric model of the double-deck vibrating screen was established using SolidWorks (2024), with its material properties set as steel. The model was subsequently imported into the simulation environment via the geometry import function of EDEM, and the unit system was unified to millimeters. Following the importation, a thorough geometric inspection of the model was performed to confirm the absence of defects such as broken surfaces or overlapping patches, thereby ensuring the validity of the contact calculations. The particle size distribution parameters adopted in the numerical model are derived from the measured results of the laboratory standard sieve tests presented in Section 2. These tests characterize the actual particle size distribution of shield muck from moderately weathered strata, providing the fundamental material input for the discrete element simulation. Built upon this parameter framework, the numerical model developed in this section is prototyped from an engineering-scale double-deck vibratory screen, and is employed to systematically investigate the effects of operational and structural parameters on screening performance. The numerical model of the double-deck vibrating screen has a screen frame with a total length of 1000 mm and a width of 300 mm. The vertical distance between the upper and lower screen decks was 140 mm, and both decks were equipped with regular square apertures. The upper screen deck had an aperture size of 3.43 mm, a bar width of 1.0 mm, and an open area ratio of approximately 60.0%, whereas the lower screen deck had an aperture size of 2.15 mm, a bar width of 0.8 mm, and an open area ratio of approximately 53.1%. Shield muck particles have complex shapes. Considering that this study primarily focuses on comparing the relative variations in screening performance under different operating parameters, the actual particles were represented as equivalent spherical discrete elements to balance computational efficiency with the requirements of multi-condition analysis. This simplification is commonly adopted in EDEM-based vibratory screening studies. The numerical model developed in this study was mainly used to analyze the relative responses of screening performance under different parameter conditions, while the particle sizes and gradation were still determined based on the laboratory test results [24]. The geometry of the double-deck vibrating screen directly affects particle trajectories, contact states, penetration behavior, and inter-deck transfer. Therefore, the main structural features, including the screen deck arrangement, inclination angle, inter-deck spacing, and discharge boundaries, were retained in the model to ensure reasonable boundary conditions for the screening process and appropriate regions for penetration statistics.

Based on the particle size distribution obtained from the laboratory screening tests, the numerical model generally followed the standard sieve sizes used in the experiments, with 9.50, 4.75, 2.36, 1.18, 0.60, 0.30, and 0.15 mm selected as representative particle sizes. Considering that the aperture size of the upper screen deck was 3.43 mm, an additional

representative particle size of 3.65 mm was introduced within the 2.36–4.75 mm size fraction to better distinguish the penetration behavior of particles on either side of the aperture size, resulting in eight particle sizes in the DEM model. For fine particles smaller than 0.15 mm, their sizes were considerably smaller than the aperture sizes of both screen decks; therefore, they were incorporated into the 0.15 mm particle size group for representation. The aperture sizes of the upper and lower screen decks were 3.43 and 2.15 mm, respectively. During screening, particles with sizes of 9.50, 4.75, and 3.65 mm could not pass through the upper screen deck. The 2.36 mm particles could pass through the upper deck but not the lower deck, whereas particles with sizes of 1.18, 0.60, 0.30, and 0.15 mm sequentially passed through both decks. After screening, particles of each size fraction were discharged through the corresponding discharge region, thereby achieving material classification. Figure 4. Structural model of the vibrating screen imported into EDEM.

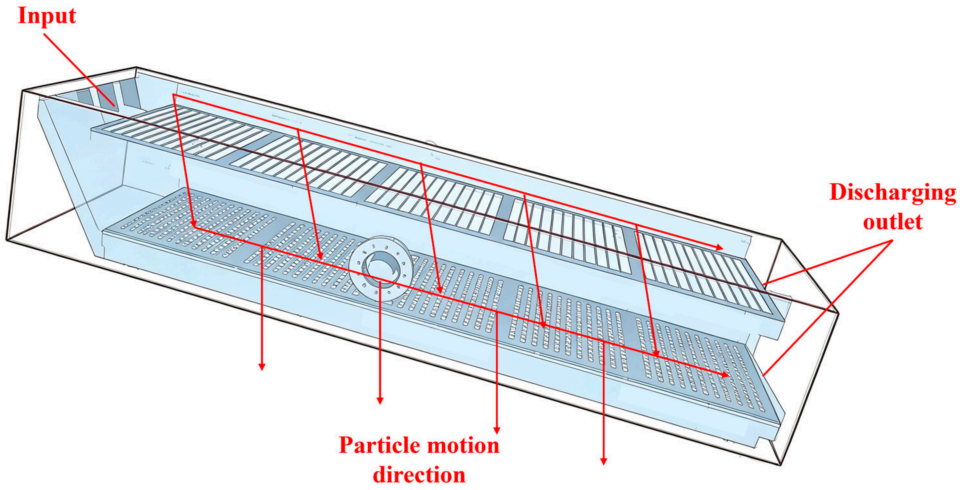


Figure 4. Structural model of the vibrating screen imported into EDEM.

Upon completing the importation of the vibrating screen geometric model, key simulation parameters—including particle material physical parameters, particle-particle and particle-wall contact parameters, particle factory generation parameters, operational parameters of the vibrating screen, and simulation duration—were configured sequentially.

The particle density and particle size distribution were determined through laboratory tests, whereas the Poisson's ratio and shear modulus were selected with reference to studies on limestone and rock particles with similar physical properties. The coefficients of restitution, static friction, and rolling friction for particle–particle and particle–screen deck interactions were determined by considering both studies on the contact parameters of granular rock materials and the commonly adopted ranges in DEM simulations of vibratory screening. Previous studies have demonstrated that the Hertz–Mindlin (no-slip) contact model can reasonably characterize the collision, friction, and rolling behaviors between particles and the screen decks during the screening of rock particles [25–28]. The physical and contact parameters adopted in this study were all within the ranges reported for similar materials, and their specific values are listed in Table 3. The same contact parameters were used for all numerical cases to ensure consistent comparisons among different combinations of operating parameters.

Following the configuration of the physical parameters, a particle factory was established within the Geometries module, and the relative mass proportions of particles with different sizes were specified according to the particle size distribution obtained from the laboratory screening tests. Based on the aperture configuration of the double-deck vibrating screen model, the aperture sizes of the upper and lower screen decks were set to 3.43 mm

and 2.15 mm, respectively. In this study, the simulated particles were divided into eight representative size fractions, with their mass proportions determined according to the measured gradation. During the simulation, particles were continuously and uniformly generated from the particle factory, with a total of approximately 3.37×10^5 particles generated, a total feed mass of 0.010 kg, and a mass feed rate of 0.001 kg/s. The particles were assigned an initial vertically downward velocity of 1.2 m/s. The relative mass proportions of particles with different sizes are listed in Table 4.

Table 3. Physical parameters of the muck particles and the screen steel.

Material	Density (kg · m^{-3})	Poisson's Ratio	Shear Modulus (Pa)
Muck particle	1800	0.30	1.0×10^7
Screen steel	7850	0.30	7.69×10^{10}

Table 4. Particle size classifications and mass proportions in the particle factory.

Particle Category	Particle Size (mm)	Mass Proportion (%)
1	9.50	0.43
2	4.75	0.70
3	3.65	11.96
4	2.36	20.37
5	1.18	25.26
6	0.60	15.40
7	0.30	17.66
8	0.15	8.22
Total	/	100

The Hertz–Mindlin (no-slip) contact model was employed to describe particle–particle and particle–screen deck contact interactions. The coefficients of restitution, static friction, and rolling friction were determined with reference to the ranges reported in DEM studies of rock particles with similar properties and vibratory screening. The specific parameters are listed in Table 5.

Table 5. Contact characteristic parameters between different materials.

Contact Type	Coefficient of Restitution	Coefficient of Static Friction	Coefficient of Rolling Friction
Particle-Particle	0.25	0.45	0.15
Particle-Screen	0.3	0.5	0.1

In this study, both the upper and lower screen decks were modeled as rigid geometries, and sinusoidal translational motion along the longitudinal direction of the screen decks was adopted. The two screen decks vibrated synchronously with the same frequency, amplitude, and phase, while their relative positions remained unchanged. Parameters such as amplitude, vibration frequency, and screen inclination angle were configured separately according to different operating conditions. Finally, the total simulation time and time step were specified prior to execution. The computational accuracy of discrete element simulations is highly dependent on the time step; an excessively large time step may lead to particle penetration during collisions, whereas an overly small time step substantially increases the computational time. In this study, 40% of the Rayleigh time step was adopted, the total simulation time was set to 10 s, and data were recorded every 0.01 s. The same simulation duration, time step, and data output interval were adopted for all operating conditions, and the screening efficiencies were consistently calculated

based on the particle mass statistics obtained over the 0–10 s simulation interval. The grid cell size of the EDEM computational domain was set to 1.00 mm, resulting in a total of 1,934,940 computational grid cells. Upon completion of the preliminary parameter configurations, the simulation was initiated. Three independent simulation runs were conducted for each operating condition, and the screening efficiency was determined by averaging the results of the three runs. The standard deviation was used to characterize the variability among repeated simulations, and the corresponding results were expressed as mean ± standard deviation. Throughout the simulation, the software automatically tracked and recorded key data, including particle trajectories and screening distributions. Upon completion of each simulation, all result files were saved for subsequent analysis.

3.1.4. Validation of DEM Contact Parameters Based on the Angle of Repose Test

To further validate the applicability of the discrete element contact parameters adopted in this study to shield muck from moderately weathered strata, an angle of repose test was conducted using the cylinder lifting method, and a corresponding EDEM numerical model was established for comparative verification. The test material was obtained from the same source and subjected to the same pretreatment procedure as that used in the preceding particle size distribution test. After washing, drying, and homogenization, the muck sample was filled into a cylindrical container without additional compaction. The cylinder used in the test had an inner diameter of 100 mm and a height of 200 mm. During the test, the cylinder was slowly lifted vertically at a constant velocity of 5 mm/s, allowing the particles to freely collapse under gravity after the lateral confinement was removed until a stable pile was formed. The natural angle of repose was then determined from the angle between the slope surface of the stable pile and the horizontal plane. The procedure of the physical angle of repose test is illustrated in Figure 5. The physical test was independently repeated three times, yielding an average angle of repose of 34.27°.

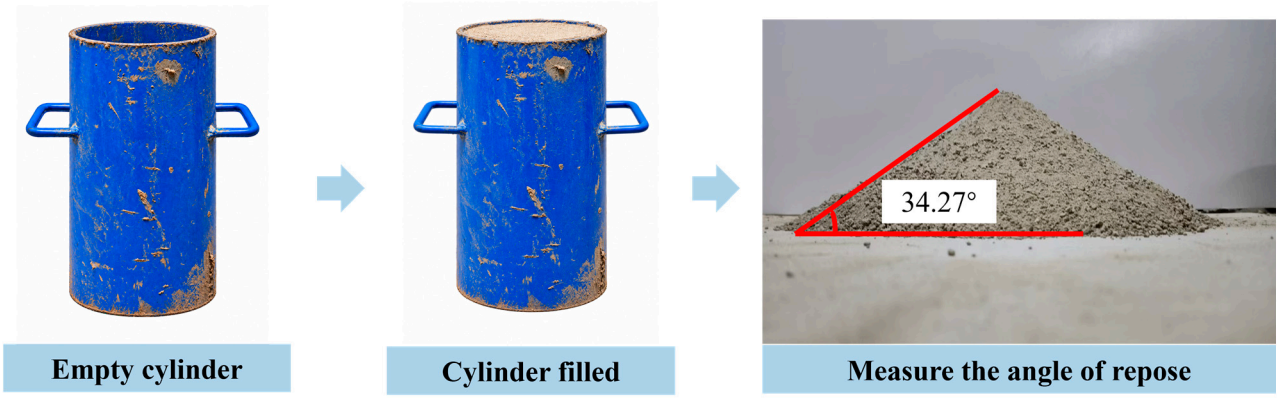


Figure 5. Experimental procedure for measuring the angle of repose of shield muck.

Based on the physical test, a corresponding discrete element model of the cylinder lifting test was further established in EDEM. The cylinder, base plate, and particle motion boundaries in the numerical model were configured in accordance with the physical test procedure. The particle size composition was kept consistent with that used in the subsequent vibratory screening model, and the physical and contact parameters determined in Tables 3 and 5 were directly adopted. Specifically, the coefficients of restitution, static friction, and rolling friction for particle–particle interactions were 0.25, 0.45, and 0.15, respectively, while the corresponding values for particle–steel interactions were 0.30, 0.50, and 0.10. To avoid the influence of artificial parameter adjustment on the validation results, these contact parameters were not further adjusted according to the physical test results during the angle of repose simulation.

At the initial stage of the simulation, the particles remained stable within the confinement of the cylinder. The cylinder was then gradually lifted in the vertical direction, allowing the particles to flow outward and rearrange under gravity. As the cylinder continued to rise, the particles progressively formed a stable conical pile. After particle motion had essentially ceased, the final slope angle of the pile was measured using the same method as that adopted in the physical test. The evolution of the particles in EDEM from the initial filling state to the stable accumulation state is illustrated in Figure 6, and the simulated angle of repose was 33.83°.

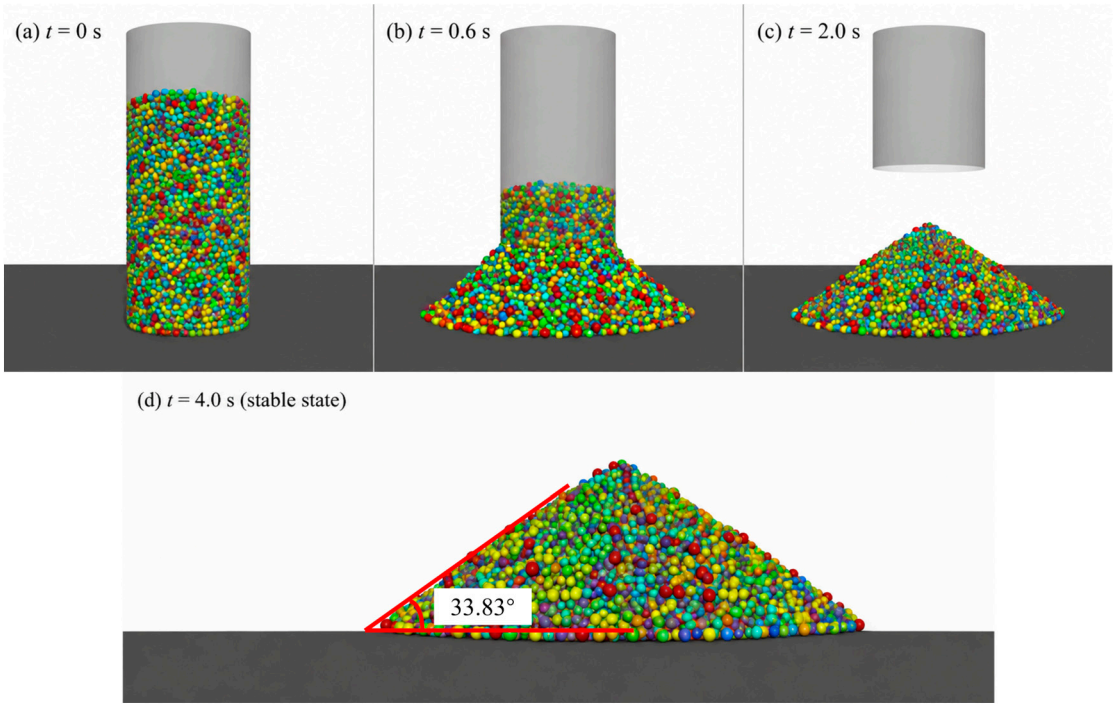


Figure 6. Particle accumulation process and stable state of shield muck in the EDEM simulation.

To quantitatively evaluate the consistency between the numerical simulation results and the physical test results, the relative deviation was adopted as the evaluation metric, which is calculated as follows:

$$RE = \frac{|\,\theta_{\mathrm{DEM}} - \theta_{\mathrm{exp}}\,|}{\theta_{\mathrm{exp}}} \times 100\% \tag{9}$$

where θ_{DEM} is the angle of repose obtained from the EDEM simulation, and θ_{exp} is the angle of repose measured in the physical test. Based on the test and simulation results, the relative deviation between the two is calculated as:

$$\Delta\theta = |\theta_{\mathrm{DEM}} - \theta_{\mathrm{exp}}| = |33.83 - 34.27| = 0.44^{\circ} \tag{10}$$

The relative deviation is calculated as:

$$RE = \frac{0.44}{34.27} \times 100\% \approx 1.28\% \tag{11}$$

The average angles of repose obtained from the physical tests and EDEM numerical simulations were 34.27° and 33.83°, respectively, with a relative deviation of 1.28%. Meanwhile, the overall shapes of the final particle piles obtained by the two methods were highly similar, indicating that the DEM contact parameters adopted in this study can reasonably reproduce the macroscopic accumulation behavior of the investigated shield muck under

gravity. It should be noted that the angle-of-repose validation primarily reflects the model's ability to reproduce static particle accumulation behavior and cannot be regarded as direct validation of the dynamic vibratory screening process. Therefore, the subsequent screening results are mainly used for relative comparisons under different operating parameters.

3.2. Screening Process of Muck Particles

A linear reciprocating vibration mode was adopted in the simulation to replicate the motion and grading process of the shield muck in actual screening equipment. To visually characterize the differences in the motion behavior of particles with various sizes, a color-coding scheme was utilized for classification and identification: cyan represents coarse particles, purple denotes medium particles, and green signifies fine particles. The simulation time started at 0 s, and the particle factory was positioned above the feed end of the upper screen deck. Particles were continuously and uniformly generated from the feed region with an initial vertically downward velocity of 1.2 m/s and subsequently entered the upper screen deck under the action of gravity.

In the model, the downstream ends of the upper and lower screen decks along the inclination direction were configured as oversize discharge outlets. During screening, particles smaller than the corresponding aperture size passed through the screen apertures into the subsequent screening region, whereas particles that did not pass through were conveyed forward along the screen deck under the combined effects of vibration and gravity and discharged from the end of the deck. Specifically, particles retained on the upper deck were discharged through the upper-deck outlet; particles that passed through the upper deck but were retained on the lower deck were discharged through the lower-deck outlet; and particles passing through the lower deck entered the collection region below. This configuration represents the actual continuous vibratory screening process, in which different particle size fractions are discharged through the oversize outlets or collected in the undersize collection region.

Under the baseline representative operating condition of the linear vibrating screen (vibration frequency: 15 Hz, amplitude: 2.0 mm, screen inclination angle: 6°), the dynamic screening process of the shield muck particles can be divided into three typical stages; the motion states of the particles at different timestamps are illustrated in Figure 7. At t = 0.38 s, the granular cluster first made contact with the upper deck screen, and no significant penetration behavior had occurred yet. At t = 0.60 s, the green fine particles and a portion of the purple medium particles, whose sizes were smaller than the upper sieve apertures, began to penetrate the upper deck onto the lower deck under the coupled effects of gravity and screen vibration. Meanwhile, the cyan coarse particles and the unpenetrated purple medium particles on the upper deck were transported along the screen toward the discharge end, driven jointly by the screen inclination angle and the vibrational inertial force. At this moment, a stable penetration material flow had formed on the upper deck, and the lower deck began to receive the medium and fine particles. At t = 5.47 s, the green fine particles on the lower screen deck had reached the discharge end, and relatively continuous particle transportation and discharge processes had been established on both the upper and lower screen decks.

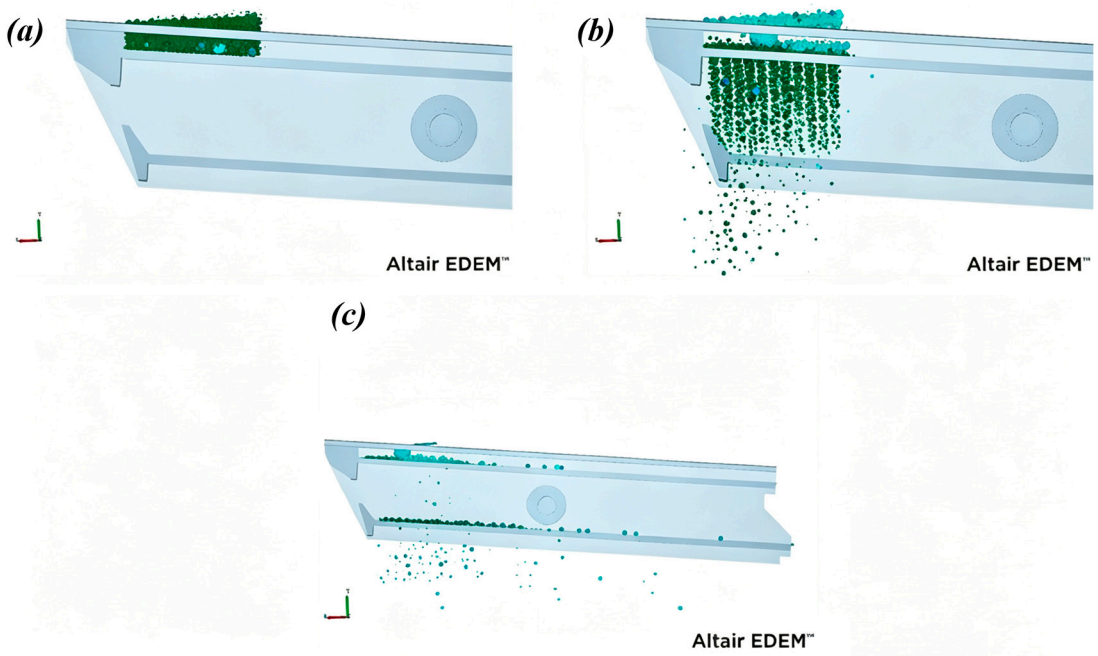


Figure 7. Motion states of particles at typical timestamps during simulation: (**a**) t = 0.38 s; (**b**) t = 0.60 s; (**c**) t = 5.47 s.

4. Analysis of Simulation Results

4.1. Evaluation Metrics for Screening Performance

Screening efficiency is a core indicator for characterizing the classification performance of a vibrating screen, directly reflecting the penetration degree of target-size particles. This metric is quantified based on the mass proportion of target-size particles that successfully penetrate the screen. In this study, a higher screening efficiency for fine-grade materials indicates that more particles smaller than the mesh size have successfully passed through the screen under vibrational excitation, demonstrating a stronger screening capacity of the model. Conversely, it implies that a portion of the target particles is retained on the screen deck, resulting in an insufficient screening process.

For the double-deck vibrating screen investigated in this study, the mass screening efficiency is employed for calculation. The calculation formulas for the screening efficiency of the two screen decks are expressed as follows:

$$\eta_1 = \frac{Q_1}{Q \cdot \alpha_1} \times 100\% \tag{12}$$

$$\eta_2 = \frac{Q_2}{Q_{2,target}} \times 100\% \tag{13}$$

where η_1 and η_2 represent the screening efficiencies of the upper and lower screen decks, respectively; Q is the total mass of the feed particles; Q_1 and Q_2 denote the masses of target-size particles passing through the upper and lower screen decks, respectively; $Q_{2,target}$ represents the total mass of target-size particles that actually enter the lower screen deck and are smaller than the lower-deck aperture size; and α_1 represents the mass proportion of target-size particles in the initial feed that are theoretically capable of passing through the upper screen deck relative to the total feed mass.

In this study, all screening performance metrics were calculated based on particle mass. The upper-deck screening efficiency was defined as the ratio of the actual mass of target-size particles passing through the upper screen deck to the mass of target-size particles in the initial feed that were theoretically capable of passing through the upper

deck. Because the upper and lower decks had different aperture sizes, their screening efficiencies corresponded to different target particle size ranges and were used separately to evaluate particle penetration through the respective decks.

To quantify the mass of particles passing through each screen deck, Geometry Bins were established beneath the upper and lower screen decks, respectively. Geometry Bin 1 was used to measure the mass of target-size particles passing through the upper screen deck, whereas Geometry Bin 2 was used to measure the mass of target-size particles that sequentially passed through both the upper and lower screen decks. During post-processing, particle masses were statistically analyzed, and the monitoring regions were spatially separated to avoid double counting between different statistical regions. Meanwhile, a mass balance check was performed by comparing the total mass of the initial feed with the sum of the particle masses in the oversize regions of each deck, the final undersize collection region, and the particles remaining within the model, thereby identifying potential mass omissions or double counting during the statistical analysis. The arrangement of the Geometry Bins used for the evaluation of double-deck screening efficiency is illustrated in Figure 8.

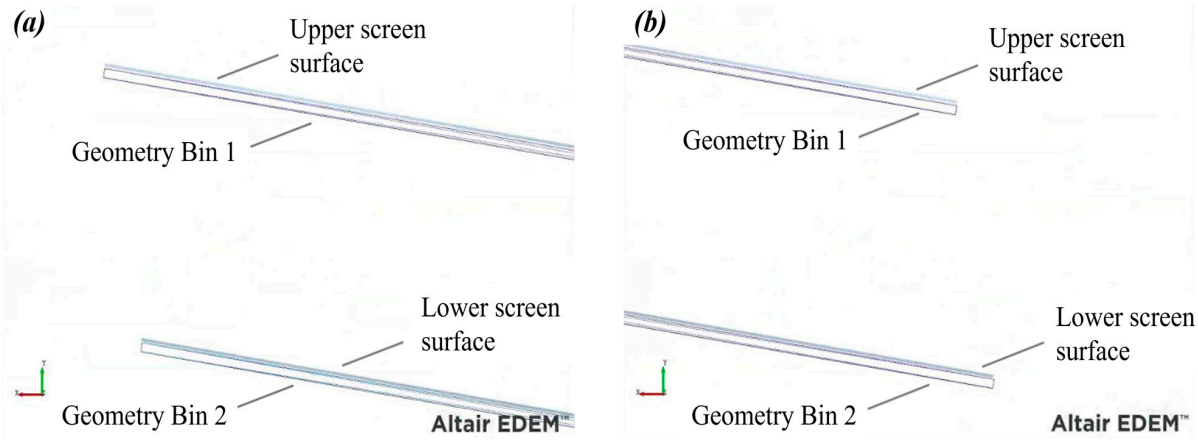


Figure 8. Schematic of the Geometry Bins setup for evaluation of double-deck screening efficiency: (**a**) arrangement of Geometry Bins relative to the upper and lower screen decks; (**b**) the same Geometry Bin arrangement viewed from another perspective.

4.2. Effects of Operational Vibration Parameters on Screening Efficiency

Vibration frequency, amplitude, and screen inclination angle are the three core parameters determining screening performance. They jointly influence screening efficiency by regulating the looseness, motion behavior, and screen residence time of the granular cluster. In this section, the single-factor control variable method was employed to systematically investigate the effects of each parameter on the screening efficiency of the double-deck vibrating screen, providing a fundamental basis for the subsequent multi-factor analysis. The vibration frequency, amplitude, and screen inclination angle were selected based on the commonly used operating parameters of vibrating screens and the screening conditions of shield muck. To balance the representativeness of the parameter ranges with the computational cost of multi-condition simulations, three representative levels (low, medium, and high) were selected for each factor. Vibration frequencies of 12, 15, and 18 Hz, amplitudes of 1.5, 2.0, and 2.5 mm, and screen inclination angles of 6°, 9°, and 12° were adopted to compare the double-deck screening performance under different operating conditions within the investigated parameter ranges.

Vibration frequency is a critical parameter governing the loose state and motion behavior of the particle cluster, directly impacting the contact probability between particles and the screen mesh, as well as the overall transport efficiency of the material. When the

vibration frequency is too low, the excitation energy of the screen surface is insufficient to effectively break the agglomeration state among particles. Consequently, it is difficult for fine-grade particles to overcome the shielding and resistance of coarse particles to migrate toward the screen surface, significantly reducing the penetration probability and preventing the screening efficiency from reaching an ideal level. Conversely, when the vibration frequency is excessively high, particles are launched off the screen surface due to excessive inertial forces, which shortens their contact time with the mesh. Meanwhile, violent vibrations tend to induce a bouncing effect in near-sieve-size particles and can even trigger chaotic jumping of the entire granular cluster, thereby diminishing the penetration opportunities and leading to a decline in screening efficiency.

As shown in Figure 9a, under the conditions of an amplitude of 2.0 mm and a screen inclination angle of 12°, the effect of vibration frequency on the screening efficiency of the double-deck vibrating screen exhibits distinct differences between the two decks. At the three investigated vibration frequencies, the screening efficiency of the upper deck first increased and then decreased, reaching 92.83% at 12 Hz, 95.16% at 15 Hz, and 94.44% at 18 Hz. In contrast, the screening efficiency of the lower deck remained generally stable at around 83%, with fluctuations of less than 1%. The differentiated responses of the upper and lower decks to vibration frequency may be related to differences in the particle size composition of the feed, particle motion states, and effective penetration conditions between the two decks. Among the three vibration frequencies investigated, 15 Hz yielded the highest upper-deck screening efficiency, whereas the lower-deck screening efficiency exhibited relatively small variations.

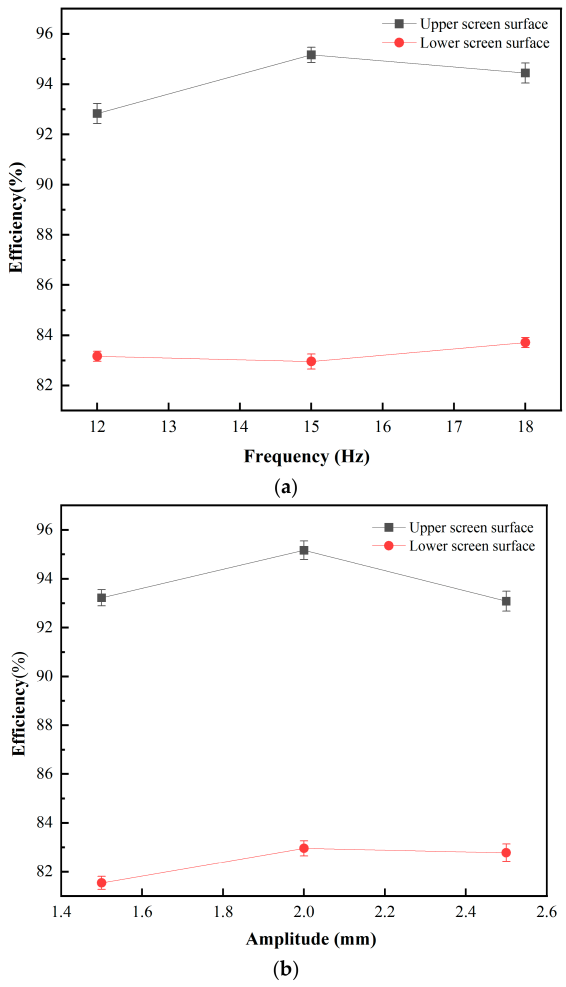


Figure 9. *Cont.*

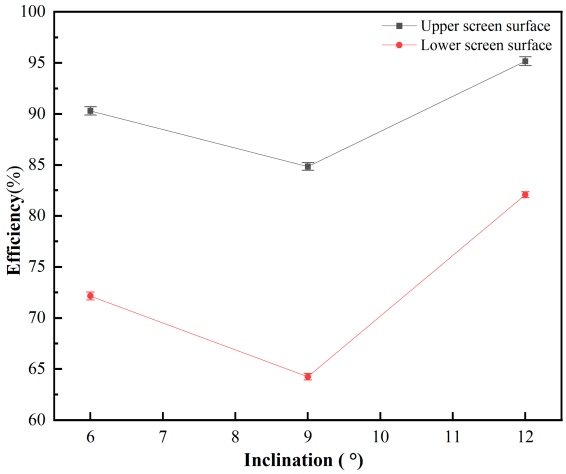


Figure 9. Effects of operational parameters on the screening efficiency of the double-deck vibrating screen (mean ± SD, n = 3): (**a**) vibration frequency; (**b**) amplitude; (**c**) screen inclination angle. (**a**) variations in screening efficiency with vibration frequency (Amplitude: 2.0 mm, Screen Inclination Angle: 12°); (**b**) variations in screening efficiency with amplitude (Frequency: 15 Hz, Screen Inclination Angle: 12°); (**c**) variations in screening efficiency with screen inclination angle (Frequency: 15 Hz, Amplitude: 2.0 mm).

Amplitude refers to the single-peak displacement of the screen box along the vibration direction during operation. In the screening process, the amplitude directly dictates the throwing intensity and segregation behavior of the muck particles on the screen surface. An appropriate amplitude allows the material bed to distribute uniformly and imparts sufficient kinetic energy to the particles to overcome inter-particle friction, thereby facilitating smooth penetration. Meanwhile, a moderate throwing intensity prevents excessive accumulation of particles on the screen deck or the occurrence of aperture blinding. When the amplitude is too low, the kinetic energy of the material is insufficient, and the particles fail to attain adequate jumping height and velocity. This results in an inadequate loosening of the material bed, obstructed penetration of fine particles, and a significant drop in screening efficiency, while exacerbating the risk of sieve blinding. Conversely, if the amplitude is excessively high, the material throwing action becomes overly intense, which shortens the contact time between the particles and the screen surface, thereby diminishing penetration opportunities. Furthermore, the violent impact induced by an over-high amplitude may aggravate particle degradation and cause fatigue damage to the mechanical structure, ultimately shortening the lifespan of the screen mesh.

As illustrated in Figure 9b, at the three investigated amplitude levels, the screening efficiencies of both the upper and lower screen decks exhibited a trend of first increasing and then decreasing. The efficiency fluctuation of the upper deck is more pronounced, whereas that of the lower deck is relatively gentle. When the amplitude increases from 1.5 mm to 2.0 mm, the granular cluster becomes looser, the segregation phenomenon is improved, and the material penetrates more thoroughly, leading to an enhancement in screening efficiency. However, after the amplitude further escalates to 2.5 mm, the excessively high throwing motion shortens the particle residence time, reduces the penetration opportunities, and intensifies the dynamic impact, which jointly result in the decline of screening efficiency.

The screen inclination angle is the angle between the screen plate plane and the horizontal plane, which directly determines the residence time of material particles on the screen surface. When the screen inclination angle increases, the component of gravity acting on the material along the downward direction of the screen surface increases. This accelerates the particle flow velocity and consequently reduces the thickness of the material

bed, thereby improving the processing capacity per unit time. However, a larger inclination angle shortens the residence time of the particle cluster on the screen surface, which diminishes the probability of fine particles obtaining penetration opportunities, thereby lowering the screening efficiency. Conversely, if the screen inclination angle is too small, the overall movement of the granular cluster becomes sluggish, and the material bed accumulates and thickens. Under this condition, fine particles are easily blocked by the coarse material layer and struggle to reach the screen surface, making the screen deck prone to blinding and leading to a reduction in screening efficiency.

As shown in Figure 9c, at the three investigated screen inclination angles, the screening efficiencies of both the upper and lower decks first decreased and then increased. For the upper screen deck, the screening efficiency was 90.30% at an inclination angle of 6°, decreased to a minimum of 84.85% at 9°, and then increased to 95.16% at 12°. Similarly, the screening efficiency of the lower deck decreased from 72.14% at 6° to 64.23% at 9°, before increasing to 82.96% at 12°. Among the three screen inclination angles investigated, 9° corresponded to the lowest screening efficiencies for both decks. When the inclination angle increased from 9° to 12°, the screening efficiencies of both the upper and lower decks improved.

As shown in Figure 9, within the specified parameter ranges, vibration frequency, amplitude, and screen inclination angle exhibited different effects on the screening efficiencies of the upper and lower decks. The upper-deck screening efficiency varied from 92.83% to 95.16% with changes in vibration frequency, corresponding to a maximum difference of 2.33 percentage points, whereas the lower-deck screening efficiency exhibited relatively smaller variations. For the screen inclination angle, the screening efficiencies of the upper and lower decks varied by 10.31 and 18.73 percentage points, respectively, across the three investigated levels, indicating that the lower deck exhibited a greater response to changes in screen inclination angle under the single-factor experimental conditions. Overall, the screening efficiencies of the upper and lower decks exhibited differentiated responses across the investigated discrete parameter levels.

4.3. Multi-Factor Analysis of Screening Efficiency

The previous section investigated the effects of individual factors on screening efficiency, demonstrating that different operating parameters exhibited distinct response characteristics when varied independently. However, in actual screening operations, parameters such as vibration frequency, amplitude, and screen inclination angle act simultaneously and jointly influence particle motion states and penetration behavior. Therefore, based on the single-factor analyses, further simulated screening experiments were conducted under different multi-factor combinations to compare the main effects of individual factors and screening performance under different parameter combinations, providing a basis for the rational selection of operating parameters.

However, in actual screening operations, parameters such as vibration frequency, amplitude, and screen inclination angle do not act in isolation. Rather, they act simultaneously and jointly influence particle motion states and penetration behavior. The response characteristics of an individual parameter may vary with changes in other parameters; therefore, configuring operating parameters solely based on single-factor analysis results has certain limitations. To further compare the screening performance under different multi-parameter combinations, simulated screening experiments were conducted based on the single-factor analyses. The main effects of the investigated factors and the screening performance under different parameter combinations were evaluated to provide a basis for rational parameter selection.

4.3.1. Orthogonal Experimental Design

In scientific research, to minimize product development costs, a substantial number of experiments must be conducted for analysis and validation. Currently, widely utilized experimental methodologies include the orthogonal design method, response surface methodology (RSM), and uniform design method. Selecting an appropriate experimental approach can effectively truncate the research and development (R&D) cycle, enhance research efficiency, and economize R&D expenses.

In this study, the orthogonal experimental design method was selected. Three operating parameters—amplitude, vibration frequency, and screen inclination angle—were designated as factors, with each factor configured at three distinct levels. A three-factor three-level orthogonal array was subsequently employed to arrange the experimental schemes, aiming to systematically investigate the main effects of individual factors and the screening performance under different parameter combinations. The maximum and minimum values of each factor were comprehensively determined with reference to relevant engineering codes and similar studies, representing the upper and lower limits of typical operating conditions. Meanwhile, the intermediate level of each factor was calculated as the arithmetic mean of its maximum and minimum values, as detailed in Table 6.

Table 6. Factor levels used in the orthogonal design.

Number	Frequency (Hz)	Amplitude (mm)	Screen Inclination Angle (°)
1	12	1.5	6
2	15	2.0	9
3	18	2.5	12

In this study, nine groups of simulation experiments were designed and conducted, with the specific parameter combinations for each test detailed in Table 7.

Table 7. Orthogonal experimental parameter matrix.

Number	Frequency (Hz)	Amplitude (mm)	Screen Inclination Angle (°)
1	12	1.5	6
2	12	2.0	9
3	12	2.5	12
4	15	1.5	9
5	15	2.0	12
6	15	2.5	6
7	18	1.5	12
8	18	2.0	6
9	18	2.5	9

4.3.2. Analysis of Orthogonal Experimental Results

Based on the numerical model of the double-deck linear vibrating screen, the particle mass statistical data corresponding to the nine groups of orthogonal experiments were derived. The screening efficiencies of both the upper and lower screen decks under each operational condition were subsequently calculated, and their evolutionary trends are illustrated in Figure 10.

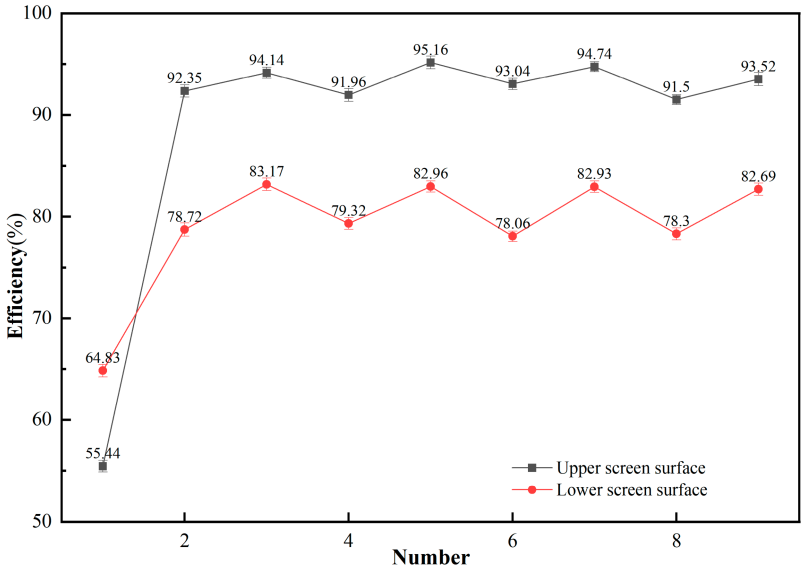


Figure 10. Screening efficiencies under different orthogonal-test conditions (mean ± SD, n = 3).

As shown in Figure 10, the upper-deck screening efficiency under operating condition 1 was 55.44%, which was significantly lower than that under the other operating conditions. This condition corresponded to a vibration frequency of 12 Hz, an amplitude of 1.5 mm, and a screen inclination angle of 6°, with all three parameters at relatively low levels within the investigated ranges. Under this parameter combination, the vibration excitation and particle transportation along the screen deck were relatively weak, which may have resulted in insufficient material-bed loosening and effective particle penetration, thereby leading to a marked reduction in upper-deck screening efficiency. Since this result corresponded to an actual operating condition included in the orthogonal experimental design, it was retained in the subsequent range analysis. It should be noted that the relatively low upper-deck screening efficiency under operating condition 1 had a certain influence on the range analysis results. Therefore, the range analysis in this study was mainly used to characterize the relative differences in the main effects of individual factors within the investigated parameter levels.

Based on the orthogonal experimental results, the range analysis method can be utilized to determine the influence weights of various operational parameters on the efficiency of the double-deck vibrating screen. The range analysis results for the upper and lower screen decks are presented in Tables 8 and 9, respectively. In Table 8, k_1, k_2 and k_3 represent the mean screening efficiencies at the different levels of each factor, while the range (R) characterizes the magnitude of the screening-efficiency response to changes in factor levels. The range analysis indicates that the factors affecting the upper-deck screening efficiency follow the order screen inclination angle > amplitude > vibration frequency, whereas those affecting the lower-deck screening efficiency follow the order screen inclination angle > vibration frequency > amplitude. The screen inclination angle exhibits a relatively large range for both decks, indicating that it has a comparatively strong influence on screening efficiency within the investigated parameter ranges.

As shown by the data in Table 9, the ranges (R) for the three factors are 5.70, 5.61, and 9.29, respectively. Therefore, the screen inclination angle has the greatest influence on the lower-deck screening efficiency, followed by vibration frequency and amplitude.

Table 8. Range analysis results of operational parameters for the upper screen deck.

	Frequency (Hz)	Amplitude (mm)	Screen Inclination Angle (°)
k_1	80.64	80.71	79.99
k_2	93.39	93.00	92.61
k_3	93.25	93.57	94.68
Range R (%)	12.74	12.85	14.69

Table 9. Range analysis results of operational parameters for the lower screen deck.

	Frequency (Hz)	Amplitude (mm)	Screen Inclination Angle (°)
k_1	75.61	75.69	73.73
k_2	80.11	79.99	80.24
k_3	81.31	81.31	83.02
Range R (%)	5.70	5.61	9.29

By correlating the tabular data with the contrastive analysis in Figure 11, the following insights can be deduced: For the upper screen deck, the order of the range values (R) for each factor is ranked as screen inclination angle (R = 14.69) > amplitude (R = 12.85) > vibration frequency (R = 12.74). This demonstrates that the screen inclination angle is the critical factor governing the sliding and penetration behaviors of the coarse particles on the upper deck. For the lower screen deck, the ranking of the range values is screen inclination angle (R = 9.29) > vibration frequency (R = 5.70) > amplitude (R = 5.61). This indicates that the sensitivity of the lower deck to various operational parameters is globally lower than that of the upper deck, yet the screen inclination angle maintains its dominant position. In summary, the screen inclination angle exerts the most significant impact on the overall screening efficiency of the double-deck vibrating screen. It should be noted that vibration frequency, amplitude, and screen inclination angle differ in their dimensions and ranges of variation. Therefore, the above ranking of their effects is applicable only to the parameter ranges and model conditions adopted in this study and should not be regarded as a generally applicable hierarchy of variables. The results can provide a reference for the preliminary selection and adjustment of operating parameters for similar double-deck vibrating screens; however, practical applications should account for equipment configuration, material properties, and site-specific operating conditions. By comprehensively comparing the screening results of the nine parameter combinations and adopting the equally weighted average of the upper- and lower-deck screening efficiencies as the overall evaluation metric, a vibration frequency of 15 Hz, an amplitude of 2.0 mm, and a screen inclination angle of 12° exhibited the best overall screening performance and can therefore be recommended as a favorable parameter combination under the model conditions investigated in this study. This result is applicable only to the discrete parameter combinations examined in this study and does not represent the global optimum in a continuous parameter space.

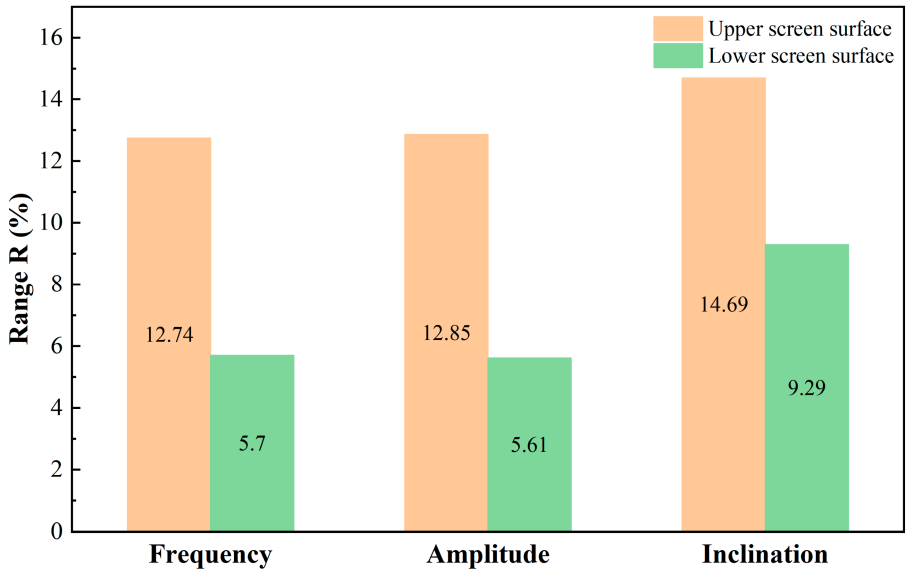


Figure 11. Range values (R) of operational parameters for the upper and lower screen decks.

This study developed a discrete element model based on spherical particles and dry materials, focusing on the relative variations in double-deck vibratory screening performance under different operating parameters. To balance computational efficiency with the requirements of multi-condition comparisons, actual particle shapes were represented by equivalent spheres, while the effects of moisture-induced cohesion, particle agglomeration, and screen aperture blockage were not considered. Therefore, the results of this study are mainly applicable to the specified dry granular system and parameter ranges. Future research will further incorporate non-spherical particle models and moisture-dependent cohesive interactions, together with physical screening tests for further model validation.

5. Conclusions

This study focuses on shield muck from moderately weathered strata and combines laboratory tests with EDEM discrete element simulations to investigate, from a particle-scale perspective, inter-deck particle migration, the evolution of screening states, and the differentiated parameter responses of the upper and lower screen decks during double-deck vibratory screening. The emphasis of this study is not only on determining suitable operating parameters but also on revealing the mechanism by which particle-state reconfiguration induced by upper-deck pre-classification affects the subsequent screening behavior of the lower deck. The main conclusions are summarized as follows:

(a) Standard laboratory screening tests showed that the coefficients of uniformity C_u and curvature C_c of the shield muck sample collected from the moderately weathered strata at Honglou Square Station on Jinan Metro Line 7 were 6.16 and 1.28, respectively, indicating a wide and continuous particle size distribution. These parameters characterize the particle size composition of the muck from the case project and can provide a reference for particle gradation analysis and discrete element modeling of shield muck under similar geological conditions.

(b) The developed DEM numerical model of double-deck vibratory screening can characterize the double-deck screening process under the specified operating conditions. The particles sequentially undergo three stages: contact with the screen decks, stratified penetration, and classified transportation and discharge. Particles smaller than the corresponding aperture sizes enter the subsequent screening or collection regions, whereas particles retained on the screen decks are conveyed to the respective dis-

charge outlets, thereby achieving the separate discharge of coarse, medium, and fine particle fractions.

(c) The double-deck screening process exhibited distinct inter-deck state changes and differentiated responses. The upper screen deck directly received a mixture with a wide particle size distribution. After selective retention and penetration on the upper deck, the particle size composition, particle quantity, and motion state of the lower-deck feed were altered, causing the upper and lower screen decks to exhibit different responses to various operating parameters, with their relative sensitivities depending on the specific parameter. For example, the lower deck exhibited a greater response to changes in screen inclination angle than the upper deck. These observations suggest that the screening state of the preceding stage may be associated with the screening performance of the subsequent stage through inter-deck particle migration.

(d) Variations in vibration frequency, amplitude, and screen inclination angle all induced non-monotonic responses in double-deck screening performance, which may be related to changes in material-bed loosening, particle transportation, and effective penetration conditions. After upper-deck pre-classification, the particle size composition and motion state of the lower-deck feed were altered, causing the two screen decks to exhibit differentiated responses to the same operating parameters. Within the parameter ranges investigated in this study, the screen inclination angle produced a relatively large variation in screening efficiency. Based on the preliminary evaluation using the numerical model and discrete parameter combinations investigated in this study, a vibration frequency of 15 Hz, an amplitude of 2.0 mm, and a screen inclination angle of 12° provided favorable overall screening performance, with upper- and lower-deck screening efficiencies of 95.16% and 82.96%, respectively. These results can serve as a preliminary reference for subsequent physical screening tests and engineering parameter selection.

(e) This study treats double-deck screening as a continuous particle evolution process characterized by inter-deck state transfer rather than as a simple combination of two independent screening stages. From a particle-scale perspective, the relationship between changes in the lower-deck feed state induced by upper-deck pre-classification and the differentiated screening responses of the upper and lower decks was analyzed. The results provide a possible particle-scale explanation for understanding the relationships between successive screening stages during the multi-stage screening of granular materials with a wide particle size distribution and offer an analytical basis for future quantitative investigations of inter-deck state transfer.

It should be noted that this study used dry shield muck after washing, drying, and homogenization. Therefore, the results are mainly applicable to the pretreated granular system and parameter ranges specified in this study, while moisture-induced cohesion, particle agglomeration, and screen aperture blockage associated with untreated shield muck under wet conditions were not considered.

Author Contributions: Methodology, Y.Y., X.W., W.H. and Y.L.; Validation, W.L.; Formal analysis, Y.L.; Resources, W.L.; Data curation, Y.Y. and W.H.; Writing—original draft, X.W., W.L. and F.L.; Writing—review & editing, X.W., W.H., Y.L. and T.L.; Visualization, T.L. and F.L.; Supervision, W.H. and Y.Z.; Project administration, T.L.; Funding acquisition, Y.Y. and Y.Z. All authors have read and agreed to the published version of the manuscript.

Funding: This article was funded by the National Natural Science Foundation of China Youth Project (No. 52308407), Shandong Provincial Natural Science Foundation Youth Fund Program (No. ZR2024QE192), and the Key Research Project of China Railway Group Limited (2022-key-13).

Institutional Review Board Statement: Not applicable.

Informed Consent Statement: Not applicable.

Data Availability Statement: The data presented in this study are available on request from the corresponding author.

Conflicts of Interest: Authors Yong Yu, Weiguo He, Tengfei Li and Wenjun Liu were employed by the company China Railway Liuyuan Group Corporation Limited. The remaining authors declare that the research was conducted in the absence of any commercial or financial relationships that could be construed as a potential conflict of interest. The authors declare that this study received funding from Key research Project of China Railway Group Limited (2022-key-13). The funder was not involved in the study design, collection, analysis, interpretation of data, the writing of this article or the decision to submit it for publication.

References

1. Yubero, M.T.; Bonet, E.; Gens, A. Analysis of local settlements due to operational EPB tunneling driving parameters: A case study of the Barcelona metro line 9 tunnel. *Sustainability* **2025**, *17*, 3966. [CrossRef]
2. EL Souwaissi, N.; Djeran-Maigre, I.; Boulange, L.; Trottin, J.-L. Effects of the physical characteristics of foams on conditioned soil's flow behavior: A case study. *Tunn. Undergr. Space Technol.* **2023**, *137*, 105111. [CrossRef]
3. Kim, T.H.; Kim, B.K.; Lee, K.H.; Lee, I.M. Soil conditioning of weathered granite soil used for EPB shield TBM: A laboratory scale study. *KSCE J. Civ. Eng.* **2019**, *23*, 1829–1838. [CrossRef]
4. Hatefi, M.H.; Arabani, M.; Payan, M.; Ranjbar, P.Z.; Keawsawasvong, S.; Jamsawang, P. The role of particle shape in the mechanical behavior of granular soils: A state-of-the-art review. *Results Eng.* **2024**, *24*, 103572. [CrossRef]
5. Yang, Y.; Xie, Z.; Wang, J.; Wang, S.; Feng, W.; Hou, X.; Yu, Y. Research on vibrating screen screening technology and method based on DEM: A review. *Min. Metall. Explor.* **2024**, *41*, 2635–2663. [CrossRef]
6. Guo, Y.; Fang, Y.; Li, X.; Jin, D.; Liu, H. Simulation of screening characterization of double-deck vibrating screen of slurry TBM tunnelling using integrated CFD-DEM-FEM. *Tunn. Undergr. Space Technol.* **2025**, *158*, 106399. [CrossRef]
7. Jaiswal, S.; Chakrabarty, A.; Atta, A.; Nag, S. Analysis of particle stratification in vibratory screening: Insights from DEM simulations. *Powder Technol.* **2025**, *465*, 121374. [CrossRef]
8. Zhang, Z.; Wan, H.; Wang, L.; Guo, Y.; Cao, J.; Xia, X. Collaborative optimization of screening efficiency and screen surface load in electromagnetic linear vibrating screen under variable frequency and amplitude. *Powder Technol.* **2025**, *2025*, 122066. [CrossRef]
9. Niu, F.; Wu, J.; Zhang, J.; Nie, Z.; Song, G.; Zhu, X.; Wang, S. Fault diagnosis method of mining vibrating screen mesh based on an improved algorithm. *Eng. Appl. Artif. Intell.* **2025**, *147*, 110343. [CrossRef]
10. Geng, R.; Yu, C.; Wang, Y.; Wang, X.; Zhang, X.; Li, R. Effect of external moisture content on screening performance of vibrating flip-flow screen and circular vibrating screen. *Minerals* **2023**, *13*, 585. [CrossRef]
11. Yang, H.; Ma, X. Research on the screening mechanisms of composite vibrating screens based on discrete elements. *PLoS ONE* **2023**, *18*, e0293205. [CrossRef] [PubMed]
12. Zhou, J.; Zhang, L.; Cao, L.; Wang, Z.; Zhang, H.; Shen, M.; Wang, Z.; Liu, F. Study on screening parameter optimization of wet sand and gravel particles using the GWO-SVR algorithm. *Processes* **2023**, *11*, 1283. [CrossRef]
13. Zhang, J.; Wang, Y.; Niu, F.; Zhang, H.; Li, S.; Wang, Y. Parameterization of multi-angle shaker based on PSO-BP neural network. *Minerals* **2023**, *13*, 929. [CrossRef]
14. Li, S.; Liu, C.; Liu, H.; He, D. Prediction and optimization of screening performance of three-deck vibrating screen based on surrogate model. *Int. J. Coal Prep. Util.* **2024**, *44*, 626–645. [CrossRef]
15. Xu, N.; Wang, X.; Lin, D.; Zuo, W. Numerical simulation and optimization of screening process for vibrating flip-flow screen based on discrete element method–finite element method–multi-body dynamics coupling method. *Minerals* **2024**, *14*, 278. [CrossRef]
16. *GB/T 6003.1-2022*; Test Sieves—Technical Requirements and Testing—Part 1: Test Sieves of Metal Wire Cloth. State Administration for Market Regulation and Standardization Administration of China: Beijing, China, 2022.
17. Chowdhury, H.; Xie, Z.; Shen, Y. Superquadric DEM study of the particle separation process in a multi-deck banana vibrating screen. *Adv. Powder Technol.* **2025**, *36*, 105003. [CrossRef]
18. Shen, G.; Xu, Z.; Dong, F.; Wang, X.; Luo, B.; Zhang, G. Effect of particle size distribution on screening efficiency of vibrating screen. *Sci. Rep.* **2025**, *15*, 39677. [CrossRef] [PubMed]
19. Hou, Y.; Li, H.; Fang, P. Theoretical study and simulation of elliptical vibrating screen with Self-Synchronous drive of double eccentric wheels. *J. Vib. Eng. Technol.* **2025**, *13*, 123. [CrossRef]
20. Yuan, L.; Sun, M.; Yan, G.; Que, K.; Wang, B.; Xu, S.; Lian, Y.; Tang, Z. Experimental Study on Loosening and Vibration Characteristics of Vibrating Screen Bolts of Combine Harvester. *Agriculture* **2025**, *15*, 749. [CrossRef]

21. Dosta, M.; Andre, D.; Angelidakis, V.; Caulk, R.; Celigueta, M.; Chareyre, B.; Dietiker, J.-F.; Girardot, J.; Govender, N.; Hubert, C.; et al. Comparing open-source DEM frameworks for simulations of common bulk processes. *Comput. Phys. Commun.* **2024**, *296*, 109066. [CrossRef]
22. Yang, X.; Yu, L.; Wang, X.; Xu, Z.; Deng, Y.; Li, H. Analysis of mesoscopic mechanical dynamic characteristics of ballast bed with under sleeper pads. *Railw. Eng. Sci.* **2024**, *32*, 107–123. [CrossRef]
23. Wang, Y.; Fan, X.; Zhao, G.; Lin, D.; Geng, R.; Xu, N.; Wang, X. Improving screening efficiency: A novel dual-drive cooperative screening system based on flexible rebound baffle and vibrating flip-flow screen coupling. *Powder Technol.* **2025**, *2025*, 121696. [CrossRef]
24. Moncada, M.M.; Rodríguez, C.G. Dynamic modeling of a vibrating screen considering the ore inertia and force of the ore over the screen calculated with discrete element method. *Shock Vib.* **2018**, *2018*, 1714738. [CrossRef]
25. Zhu, C.; Long, H.; Peng, Z.; Wang, X.; Chen, X.; Tian, Z.; Fan, H. Research on the optimization efficiency of secondary vibrating screening based on EDEM simulation. *Sci. Rep.* **2026**, *16*, 6746. [CrossRef] [PubMed]
26. Qin, R.; Fang, H.; Liu, F.; Xing, D.; Yang, J.; Lv, N.; Chen, J.; Li, J. Study on physical and contact parameters of limestone by DEM. In *IOP Conference Series: Earth and Environmental Science*; IOP Publishing: Bristol, UK, 2019; Volume 252, p. 052110.
27. Harzanagh, A.A.; Orhan, E.C.; Ergun, S.L. Discrete element modelling of vibrating screens. *Miner. Eng.* **2018**, *121*, 107–121. [CrossRef]
28. Dong, K.J.; Wang, B.; Yu, A.B. Modeling of particle flow and sieving behavior on a vibrating screen: From discrete particle simulation to process performance prediction. *Ind. Eng. Chem. Res.* **2013**, *52*, 11333–11343. [CrossRef]

Disclaimer/Publisher's Note: The statements, opinions and data contained in all publications are solely those of the individual author(s) and contributor(s) and not of MDPI and/or the editor(s). MDPI and/or the editor(s) disclaim responsibility for any injury to people or property resulting from any ideas, methods, instructions or products referred to in the content.